Extraction of Doping Density Distributions from C-V Curves

Hartmut F.-W. Sadrozinski
SCIPP, Univ. California Santa Cruz, Santa Cruz, CA 95064 USA

1. Connection between C, Neff, V

Start with Poisson equation

$$\frac{d^2V}{dx^2} = -\frac{e}{\varepsilon} N_{eff} \qquad (1)$$

and the equation for capacitance of a parallel capacitor

$$C = \varepsilon \frac{A}{x} \qquad (2)$$

. where x is the thickness of the depleted region. We measure C-V, i.e. the capacitance as a function of voltage, which using eq. 2 can be turned into V(x). According to eq. 1, differentiating this function twice results in the depletion voltage.

Successive approximation works quite well: divide the capacitor of thickness d into slabs of equal thickness t, which each have a capacitance

$$C_t = C_o \frac{d}{t}. \qquad (3)$$

The reciprocal of these constant capacitances can be added up to make up the capacitance measured and the corresponding voltages $\Delta_t V(x)$ across the capacitors are adjusted to match the observed C-V curve. Assuming that the doping density does not change across the distance t, the voltage $\Delta_t V(x)$ can be expressed in term of the local doping density

$$\frac{dV(x)}{dx} = -\frac{e}{\varepsilon}\int_0^x N_{eff}(x)dx \qquad (4)$$

$$\Delta_t V(x) = -\frac{e}{\varepsilon}\int_x^{x+t}\int_0^x N_{eff}(x)dx'dx = -\frac{e}{2\varepsilon}N_{eff}(x)((x+t)^2 - x^2)) = -\frac{e}{\varepsilon}N_{eff}(x) * x * t \qquad (5)$$

Need good fits for C vs. V curves for this, and a student is working on this.

2. Simulations using Neff distributions

One approach is to assume a trial Neff distribution and adjust the parameters such that the simulated C-V curves fit the experimental ones.

$$\frac{dV(x)}{dx} = -\frac{e}{\varepsilon}\int_0^x N_{eff}(x)dx = -\frac{e}{\varepsilon}N_{eff}(1) * (x - xx0) + E_0$$

$$E(0) = E_0$$

$$E_c = -\frac{e}{\varepsilon}N_{eff}(1) * (xx1 - xx0) + E_0$$

$$E_0 = +\frac{e}{\varepsilon}N_{eff}(1) * (xx1 - xx0) + E_c$$

$$V(x) = -\frac{e}{2\varepsilon} N_{eff}(1) * [(x)^2 - (xx0)^2] - \frac{e}{\varepsilon} N_{eff}(1) * xx0 * [x - xx0] + E_0 * [x - xx0] - V_0$$

For un-irradiated detectors or detectors where the doping densities are uniform or at least monotonic functions of the depth, this is a straight forward procedure: one slowly increases the depletion depth with a step size of about one micron, and calculates the corresponding fields and voltages depending on the trial Neff distributions.

For trial distributions, we follow the model from Fig. 3.b of our Carmel paper (M. Bruzzi et al.) shown in Table I and Fig. 1, where three regions with constant Neff's are defined; one in front with N_{eff}(front), a constant field region in the center (N_{eff}=0) and one with the opposite sign in the back, N_{eff}(back). These distributions were derived from TCT data of b-type MCz detectors irradiated to higher fluences. The simulation varies the boundaries of these three regions and the value of the Neff's.

Table I: Trial Neff Distributions

Neutrons			Protons		
x [um]	E [V/cm]	Neff [cm-3]	x [um]	E [V/cm]	Neff [cm-3]
0	5000	1.51E+12	0	24000	7.11E+12
150	1500	1.51E+12	200	2000	7.11E+12
190	1500	-1.88E+13	240	2000	-8.76E+12
299	33000	-1.88E+13	299	10000	-8.76E+12

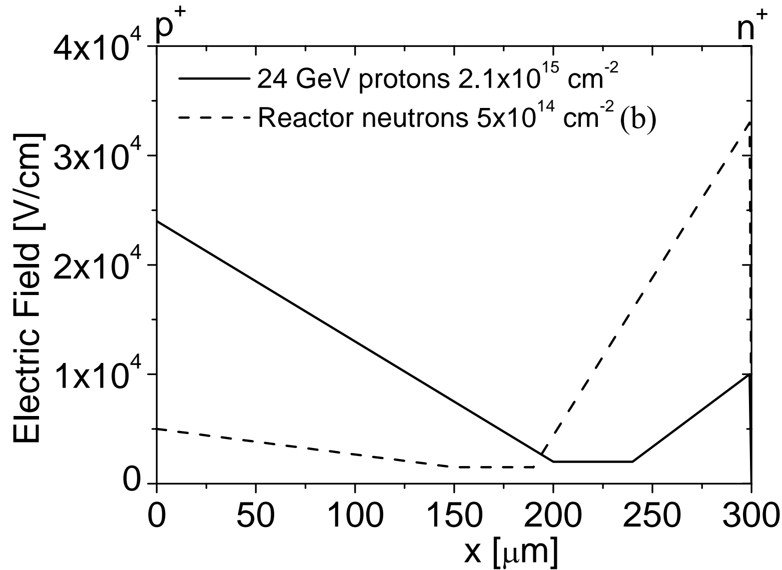

Fig. 1 Electric field profile as determined by TCT in n-type MCz silicon after irradiation with 24 GeV protons up to $2x10^{15}cm^{-2}$ and with $5x10^{14}cm^{-2}$ 1MeV neutrons.

For irradiated detectors, which might exhibit a double junction (DJ), one can try to start depletion from both sides. The question is then which step size to choose on the two sides. The only choice of step size which let to a reasonable agreement between

simulation and data was that the step size at the back contact Δx_b was reduced in the ratio of the respective Neff's with respect to the front side Δx_f:

$$\Delta x_b = N_{eff}(front) / N_{eff}(back) * \Delta x_f$$

Since in all cases considered the back side Neff was much larger, the results were consistent with starting the depletion only from the front. In many cases, starting the depletion from the front leads to better fits of the data, as shown in Fig. 2. The extracted distributions of the doping densities are qualitatively quite similar, and in the following we will consider the simulations starting from the front only.

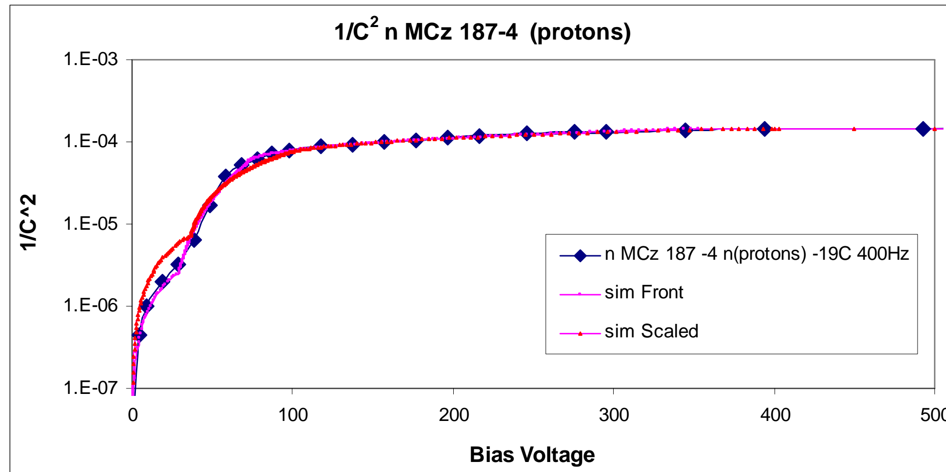

Fig. 2 Logarithmic plot of the $1/C^2$ – V distribution of a n-type MCz silicon detector after irradiation with 24 GeV protons up to $1.4x10^{15}cm^{-2}$ with simulations starting either at the front or both on the ftont and the back ("scaled").

3. Devices

We used the C-V curves of the six SMART SSD shown in Table II. The un-irradiated p-type FZ SSD 68-1 was used to verify that the procedure resulted in the expected distributions based on a uniform Neff.

Table II: SMART SSD used

SSD	Wafer	Fluence [neq/cm^{-2}]	Temperature [^{o}C]	Frequency [Hz]	CCE
187-2 187-2	n MCz 300 µm	$1.4*10^{14}$ protons	-10	400	Yes Yes
253-4	p MCz 300 µm	$\sim 1.4*10^{14}$ protons	-10	400	Yes
66-8	p MCz 300 µm	$\sim 4*10^{14}$ neutrons	-20	250	Yes
1256-3	n FZ 300 µm	$\sim 4*10^{14}$ neutrons	-20	250	
14-5	p FZ 200 µm	$\sim 4*10^{14}$ neutrons	RT	10,000	

68-1	p FZ 200 µm	Pre-rad	RT	10,000	

4. Results

4.1 C-V Normalisation:

Fig. 3 shows that the normalization of the capacitance is well understood: we get agreement between the different SSD at depletion. The two p MCz detectors with roughly the same fluence in neutrons and protons agree very well in the limited voltage range where they can be compared: this opens up the possibility to make predictions for depletion profile even for detectors which show early breakdown, once we gain more experience with the C-V curves. The p-type FZ detectors have 200 µm thickness, and it will be interesting to compare the LTLF data of 14-5 with the pre-rad data of 68.1.

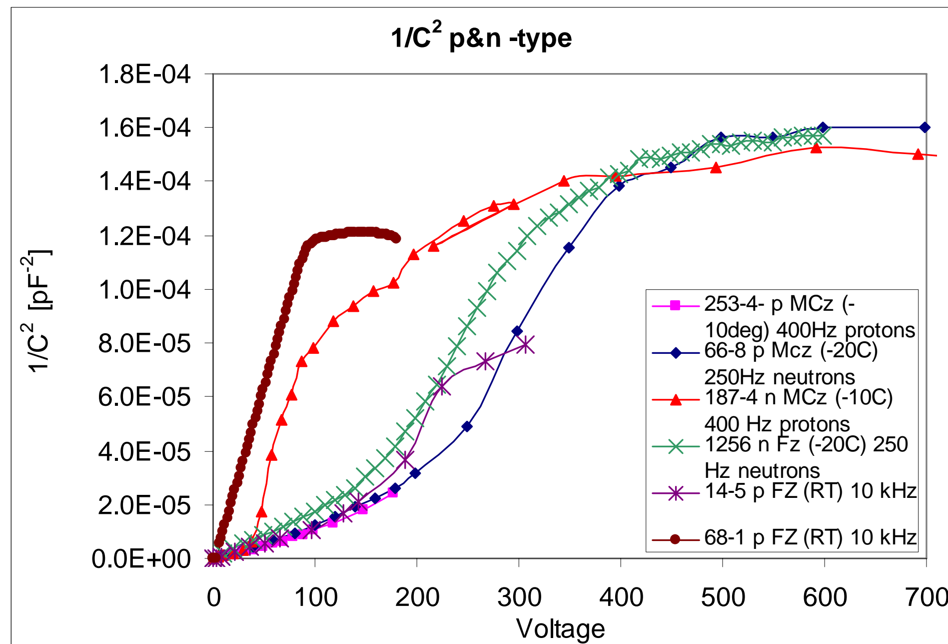

Fig. 3 Measured $1/C^2 - V$ curves at the optimal frequencies for the temperatures selected.

4.2 Simulation Results

Fig. 4 shows the results on the simulations of the two MCz detectors which could be fully depleted. The agreement between data and simulations are quite good, and the fits could be improved even more by using a double-junction model with two non-uniform Neffs. As control, the simulation of the un-irradiated p-type FZ detector 68-1results in a straight-line $1/C^2$ behavior and a constant doping density of $3.02*10^{12}$ cm^{-3}.

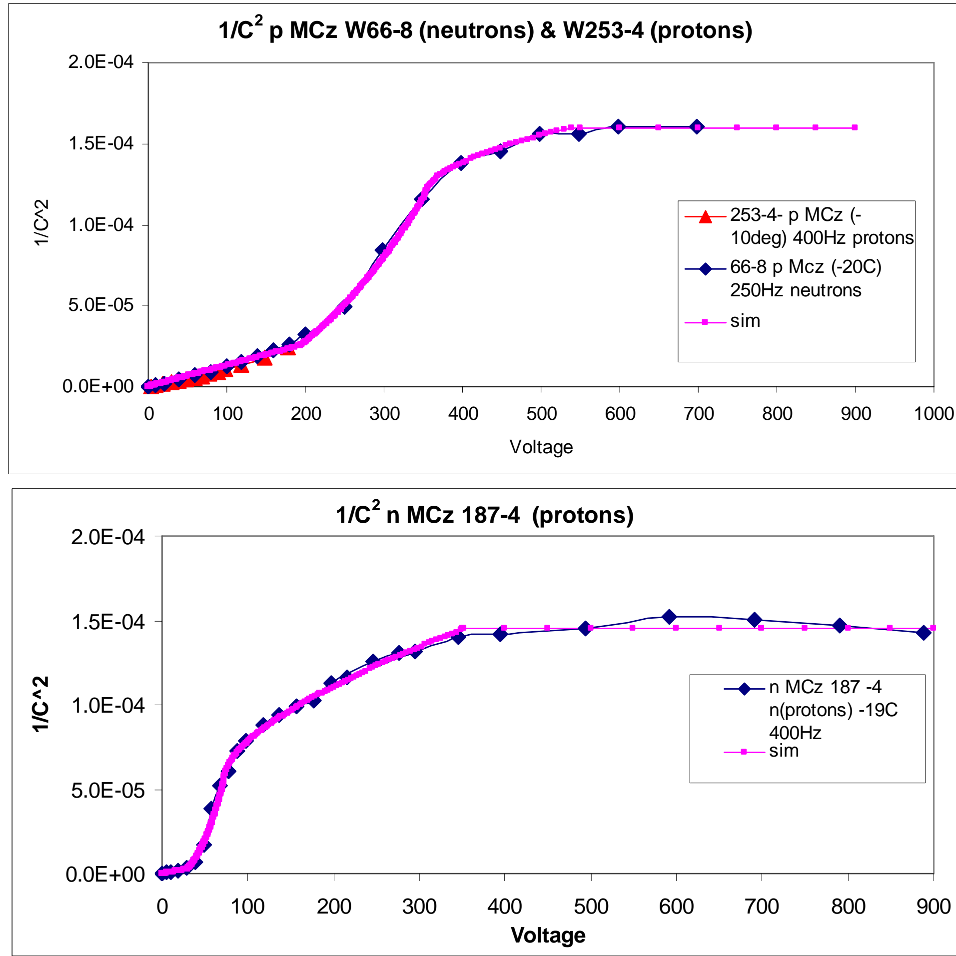

Fig. 4 Measured and simulated $1/C^2$ curves. The fits are quite good, but could be improved using a double-junction model with two non-uniform Neffs,

The fits yield distributions of the effective donor concentration in the assumed double junction model. They are shown in Table III and Fig. 5. A comparison of the electric field profiles for the two MCz detectors is shown in Fig. 6. As in Fig. 1, a double junction is clearly seen with a relative low-filed region in the detector center, indicating a very high resistivity bulk. The relative strength of the front to back junctions is clearly different in the two samples, and we have to await the results on n MCz irradiated with neutrons to decide if this is a property of the material or due to the irradiating particle species as suggested by the extraction of the filed by TCT (Fig. 1). The n-type MCz detector shows a much larger extend and much lower strength of the electrical field in the intrinsic bulk.

Table III: Simulated Neff Distributions

187-2 n MCz (protons)			66-8 p MCz (neutrons)		
x [um]	E [V/cm]	Neff [cm-3]	x [um]	E [V/cm]	Neff [cm-3]
0	18,000	2.4E+13	0	44,000	1.8E+13
40	3,000	2.4E+13	119	11,500	1.8E+13
183	3,000	-2.7E+13	257	11,500	-1.3E+14
300	46,000	-2.7E+13	300	23,000	-1.3E+14

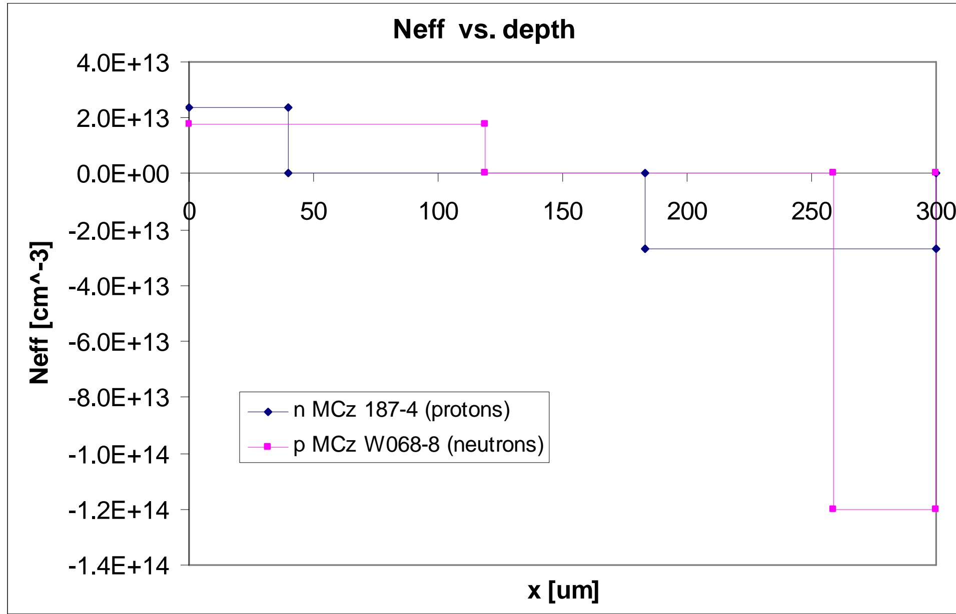

Fig. 5 Extracted doping density profile Neff vs. detector depth for both n- and p-type MCz detectors.

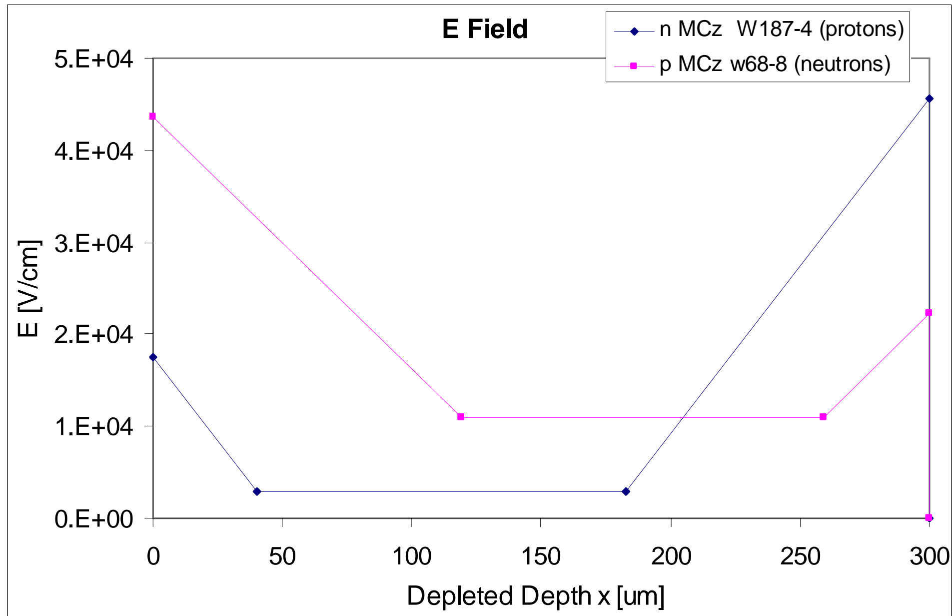

Fig. 6 Extracted electric field distribution vs. detector depth for both n- and p-type MCz detectors. The relative size of the fields at front (x ≈ 0) and back. (x ≈ 300) is different fro n-type and p-type.

4.3 Charge Collection

From the fits the depletion characteristics of the detectors can de extracted. The depleted depth is proportional to the reciprocal capacitance. Fig. 7 shows the depth of the depleted region as a function of voltage for the investigated p-type n-type, and describes the same data as Fig. 3. The most striking feature is that the n-type MCz has very

different depletion characteristics from all other wafer types. We will soon have data from all detector types, irradiated with both neutrons and protons, which will allow us to determine the dependence of the depletion characteristics on wafer and particle type.

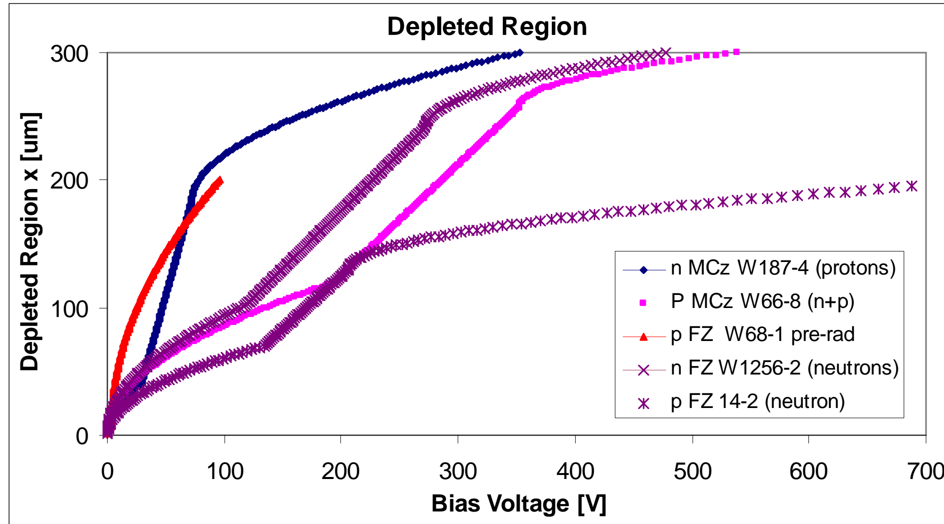

Fig. 7 Depletion characteristics extracted from the fits. The depleted region is proportional to the reciprocal capacitance.

A critical test of the simulation procedure is the comparison of the C-V data with charge collection (CC-V). Good agreement of CC-V with the expectation (Fig. 7) would allow substituting relatively easy and fast electrical measurements like C-V for the much more involved charge collection procedure to characterize the performance of irradiated detectors. Differences between C-V and CC-V might be interpreted as an indication for trapping.

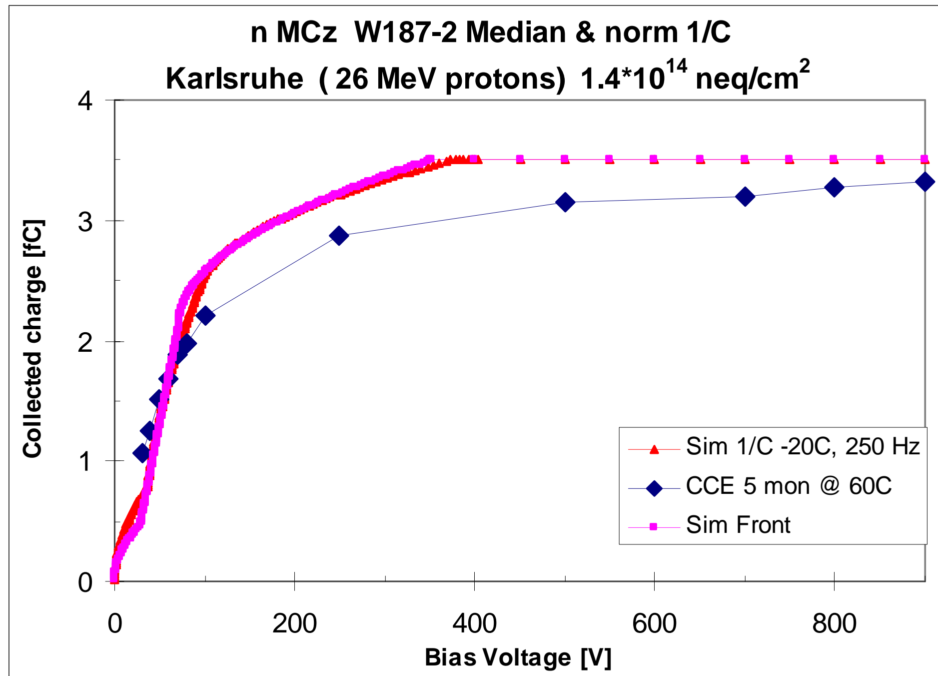

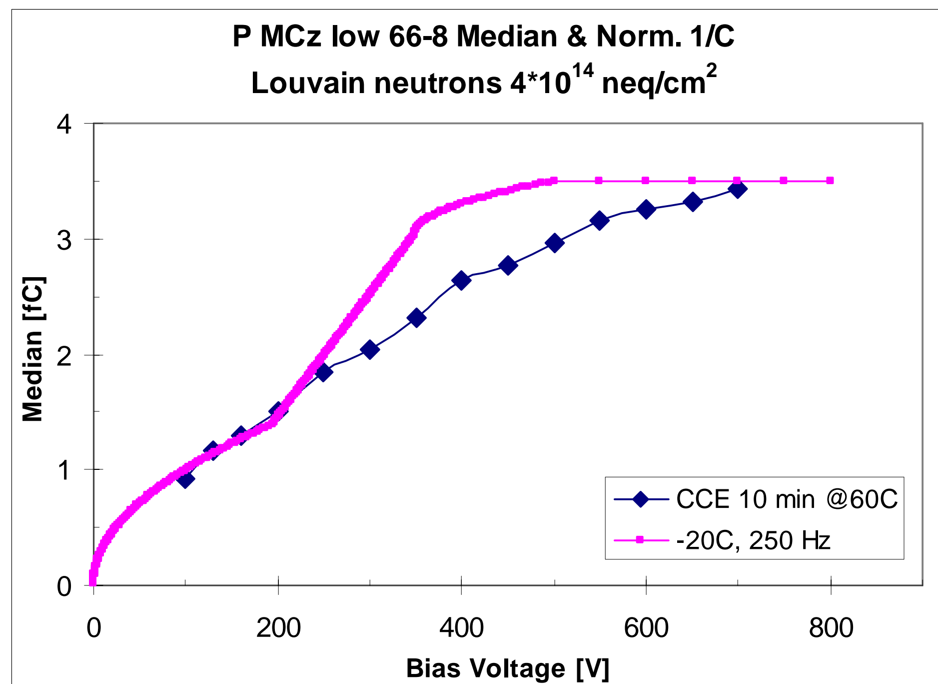

Fig. 8 Measured median charge collected vs. bias voltage (CC-V) and the prediction from the fits to the C-V data. The normalization between the different curves is accurate to about 10%. The difference between the CC-V and reciprocal C-V curves might be explained by trapping in the neutral bulk.